ACS Energy LETTERS

Cite This: ACS Energy Lett. 2019, 4, 1098−1105

http://pubs.acs.org/journal/aelccp

LETTER

Directing Selectivity of Electrochemical Carbon Dioxide Reduction Using Plasmonics

Erin B. Creel,[†,‡,§] Elizabeth R. Corson,[†,∥] Johanna Eichhorn,[†] Robert Kostecki,[†,⊥] Jeffrey J. Urban,[†,§] and Bryan D. McCloskey*[,†,∥,⊥]

[†]Joint Center for Artificial Photosynthesis, Lawrence Berkeley National Laboratory, Berkeley, California 94720, United States

[‡]Department of Chemistry, University of California, Berkeley, California 94720, United States

[§]The Molecular Foundry, Lawrence Berkeley National Laboratory, Berkeley, California 94720, United States

[∥]Department of Chemical and Biomolecular Engineering, University of California, Berkeley, California 94720, United States

[⊥]Energy Storage and Distributed Resources Division, Lawrence Berkeley National Laboratory, Berkeley, California 94720, United States

Supporting Information

ABSTRACT: Catalysts for electrochemical carbon dioxide reduction in aqueous electrolytes suffer from high energy input requirements, competition with hydrogen evolution from water reduction, and low product selectivity. Theory suggests that plasmonic catalysts can be tuned to selectively lower the energy barrier for a specific reaction in a set of competitive reactions, but there has been little experimental evidence demonstrating plasmon-driven selectivity in complicated multielectron electrochemical processes. Here, the photoactivity at a plasmonically active silver thin film electrode at small cathodic potentials selectively generates carbon monoxide while simultaneously suppressing hydrogen production. At larger cathodic potentials, the photoactivity promotes production of methanol and formate. Methanol production is observed only under illumination, not in dark conditions. The preference of the plasmonic activity for carbon dioxide reduction over hydrogen evolution and the ability to tune plasmonic activity with voltage demonstrates that plasmonics provide a promising approach to promote complex electrochemical reactions over other competing reactions.

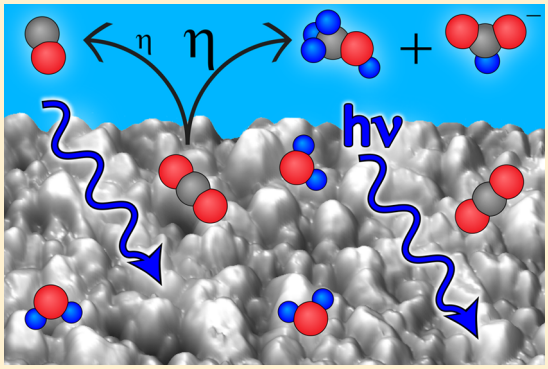

The rapid increase in atmospheric carbon dioxide (CO_2) concentration due to the burning of fossil fuels is the primary cause of atmospheric and oceanic warming, decreasing snow and ice cover, and rising sea levels over the last 3 decades.[1] The need to lessen the impacts of climate change is driving the need to mitigate CO_2 levels and find an alternative fuel source. One possible component of this approach, electrochemical reduction of CO_2, converts water and waste CO_2 into a variety of value-added chemicals such as carbon monoxide (CO), methanol, and ethylene. However, CO_2 reduction suffers from the high overpotentials needed to overcome sluggish kinetics, low selectivity for desired products, and unfavorable competition with water reduction (the hydrogen evolution reaction (HER)).[2,3] Challenges limiting energy efficiency and selective product formation must be addressed to make CO_2 reduction a viable energy storage solution.

Plasmonic catalysis may bypass the shortcomings in traditional "dark" catalysis for multielectron reductions because of its ability to couple light energy into surface chemistry.[4] Surface plasmon resonance (SPR) in nanostructured metals has been shown to increase reaction rates in a variety of reactions,[5−8] including gas-phase CO_2 reduction.[9,10] However, the effect of SPR on the Coulombic efficiency and selectivity of electrochemical CO_2 reduction product(s) has not been extensively explored despite the promising improvements in selectivity seen in purely plasmonic photocatalytic (without voltage bias) CO_2 reduction.[11]

SPR is the incident-light-stimulated collective oscillation of conduction electrons at the interface between a material with positive permittivity such as water or air and a material with negative permittivity such as a metal. This phenomenon is induced by strong, resonant light absorption at a wavelength of light dictated by the size, shape, dielectric environment, and composition of the nanostructure. The plasmon resonance

Received: March 7, 2019
Accepted: April 12, 2019
Published: April 12, 2019

DOI: 10.1021/acsenergylett.9b00515
ACS Energy Lett. 2019, 4, 1098−1105

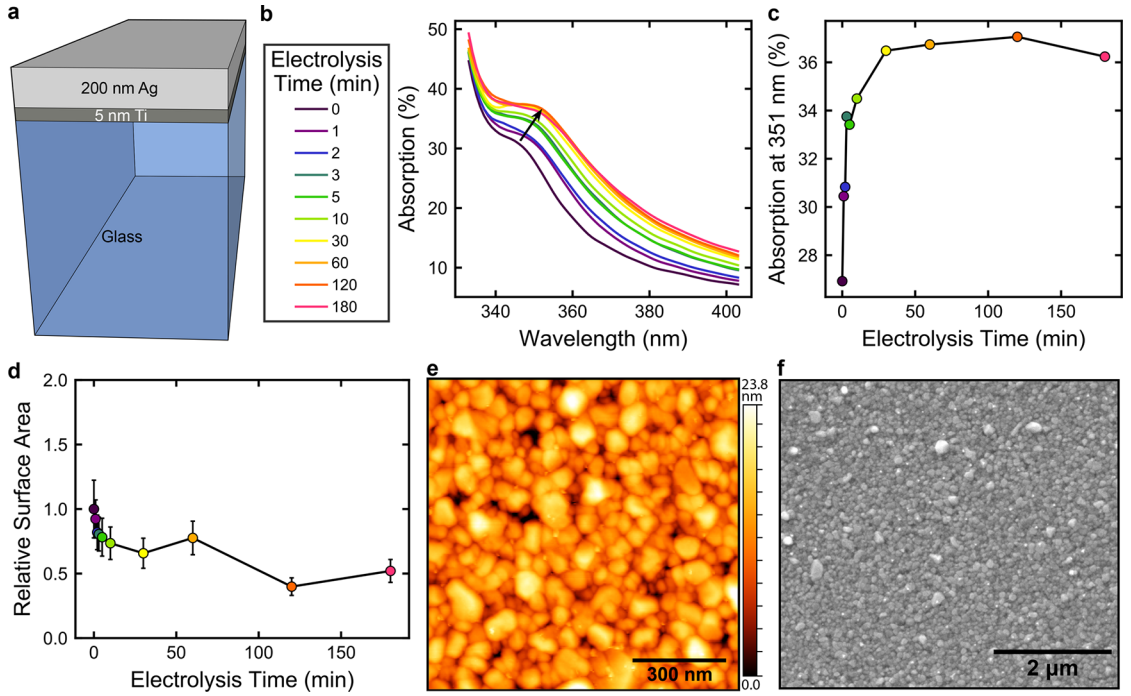

Figure 1. Silver thin film cathode characterization. (a) Diagram of a silver cathode showing e-beam-deposited 200 nm silver on 5 nm of titanium on a glass slide. (b) Evolution of the UV−visible absorption spectra of an electrode after CO_2 reduction at −1.1 V_{RHE} for various times. (c) Evolution of the absorption of an electrode at 351 nm after biasing at −1.1 V_{RHE} in CO_2-saturated 1 M $KHCO_3$ for various times. Absorption is calculated as 100%−%*R* where %*R* is the total reflection measured by an integrating sphere. (d) Evolution of the electrochemical surface area measured by double-layer capacitance normalized to the as-deposited electrode after biasing at −1.1 V_{RHE} for various times. (e) AFM topographic image of the electrode surface after biasing at −1.1 V_{RHE} for 45 min. (f) SEM image of the electrode surface after biasing at −1.1 V_{RHE} for 45 min.

produces a dramatic enhancement of the local electric field on the nanostructure surface and excites "hot" electrons and holes as the initial plasmon oscillation decays. Plasmonic catalysis theory has predicted that plasmonic catalysts can be tuned such that hot carriers can be selectively injected into specific adsorbates to promote a desired reaction over other competing reactions.[12−15] However, experimental evidence of plasmon-induced product selectivity changes in electrochemical systems is limited.[16−18] Furthermore, the role of using an applied voltage in photoelectrochemical plasmonic catalysis has received little attention as a strategy for altering product selectivity and reactivity. While some research on plasmonic photoelectrochemical CO_2 reduction at a single potential has shown plasmonic enhancement of CO production,[19−21] there have been no studies characterizing plasmonic photoelectrochemical CO_2 reduction at a range of voltages.

We use a silver electrode without a supporting absorber to probe the effect of plasmonic excitation on CO_2 reduction at several potentials. Silver is an ideal heterogeneous catalyst for plasmonic electrochemical reduction of CO_2 because of its well-understood "dark" CO_2 electrocatalytic performance,[2,22] and the resonant excitation of silver surface plasmons occurs upon illumination with near-UV−visible light irradiation at 340−400 nm (3.1−3.6 eV).[23] Moreover, due to the electronic band structure of silver, SPR is predicted to generate high-energy hot electrons,[24] making this metal appropriate for a reduction reaction study. Many transition metals are poor CO_2 reduction catalysts because they produce primarily hydrogen, but silver electrodes promote CO production at ambient temperature and pressure with reasonable CO formation selectivity over hydrogen evolution, albeit at large over-potentials (approximately 1 V) in near-neutral-pH aqueous electrolyte.[2,22] Silver cathodes also produce small amounts of formate at potentials more cathodic than −0.6 V versus the reversible hydrogen electrode (V_{RHE}) and exceedingly small amounts of methanol, ethanol, and methane at highly cathodic potentials (more cathodic than −1.3 V_{RHE}).[22]

Here, we show that the plasmonic activity over a polycrystalline silver thin film electrode is significant and selective for CO_2 reduction while suppressing hydrogen evolution at low applied cathodic potentials. Hydrogen production is also suppressed under illumination of a silver cathode in CO_2-free (Ar-saturated) electrolyte, resulting in a decrease in activity. An illuminated silver electrode generates CO at >90% Faradaic efficiency at much lower overpotentials than an unilluminated silver electrode. Methanol production is not observed without illumination at cathodic potentials down to −1.2 V_{RHE}, but methanol production under illumination is produced at 0.1−2% Faradaic efficiency between −0.8 and −1.1 V_{RHE}, which is an unprecedented methanol Faradaic efficiency for silver cathodes. Interestingly, the enhancement in CO production is observed only at −0.8 V_{RHE} and potentials more anodic, while the methanol production occurs only at −0.8 V_{RHE} and potentials more cathodic. This is the first known example of using applied voltage to control the product selectivity of plasmonic-driven reactions, indicating that voltage bias is an important variable in tuning and understanding plasmonic selectivity in complex electrochemical reactions. Additionally, the combined enhancement of CO_2 reduction and suppression of hydrogen evolution via plasmonic catalysis may be an important breakthrough in directing selective aqueous electrochemical CO_2 reduction.

DOI: 10.1021/acsenergylett.9b00515
ACS Energy Lett. 2019, 4, 1098−1105

Synthesis and Structural Characterization of Silver Thin Films. We fabricated the silver photocathodes by electron-beam (e-beam) evaporating silver onto a glass slide substrate using titanium as an adhesion layer (Figure 1a) followed by electrochemical conditioning of the surface at −1.1 V_{RHE} in aqueous CO_2-saturated potassium bicarbonate ($KHCO_3$) electrolyte. Electrochemical conditioning of the electrode was necessary due to the evolution of the electrode's optical properties and morphology with CO_2 electrolysis. The as-deposited silver film exhibited a weak absorption peak at 346 nm (Figure 1b) that corresponds to the silver SPR.[23] After only 1 min of CO_2 electrolysis, the absorption of the rinsed and dried cathode increased across the spectrum, with the plasmonic peak broadening and red-shifting. The plasmonic absorption peak continued to widen and move toward larger wavelengths with further CO_2 electrolysis until it reached a steady state between 30 and 60 min of electrolysis with an absorption maximum at 351 nm (Figure 1b,c). No change in the plasmonic absorption occurred when the electrode was immersed in electrolyte without applied bias. We hypothesized that the large applied voltage caused the silver nanostructures on the rough evaporator-deposited surface to ripen into larger, more stable nanostructures.[25,26]

To test this hypothesis, we measured the electrochemical double layer capacitance as a proxy for electrochemical surface area (ECSA) at various intervals over the electrolysis time (Figure S1). The ECSA decreases then stabilizes over electrolysis time (Figure 1d), consistent with the coarsening hypothesis from absorption measurements.

Scanning electron microscopy (SEM) images and atomic force microscopy (AFM) topographic images (Figures 1e,f, S2, and S3) show nodule-like features of 10−100 nm on the electrode surface both before and after 45 min of electrolysis even though the electrode surfaces appear mirror-like to the naked eye. AFM root-mean-squared (RMS) surface roughness measurements before and after electrochemical conditioning—6.0 and 4.4 nm, respectively—indicate a slight decrease in surface roughness, matching the ECSA measurements. The AFM topographic images indicate that the grain size distribution broadens slightly, increasing the population of both large and small features, after electrochemical conditioning (Figure S2e). However, this difference is difficult to observe when comparing the SEM and AFM images, indicating that the morphology differences that result in the plasmonic activity are likely too subtle to be detected by examination of these images.

CO_2 Electrochemical Reduction Product Measurements. The gaseous products of CO_2 reduction over the silver cathode were measured by an in-line gas chromatograph (GC) while applying a constant voltage.[21] The liquid products were measured by proton nuclear magnetic resonance (^{1}H NMR) of the electrolyte after the electrochemical measurement was complete. The cathode was continuously illuminated from the front with 170 mW cm^{-2} incident light intensity from a 365 nm light-emitting diode (LED), which was selected given its proximity in energy to the plasmon resonance peak (351 nm, Figure 1b) of our conditioned silver electrodes, or left unilluminated for the "dark" control. No high-power LEDs (2−3 W cm^{-2}) are available below 365 nm, limiting the range of photon energies studied here to the visible spectrum, which is interesting for solar-driven processes. Our electrolysis cell was specifically designed to ensure precise temperature control, and all measurements, both illuminated and in the dark, were performed at 22 ± 0.1 °C.[21]

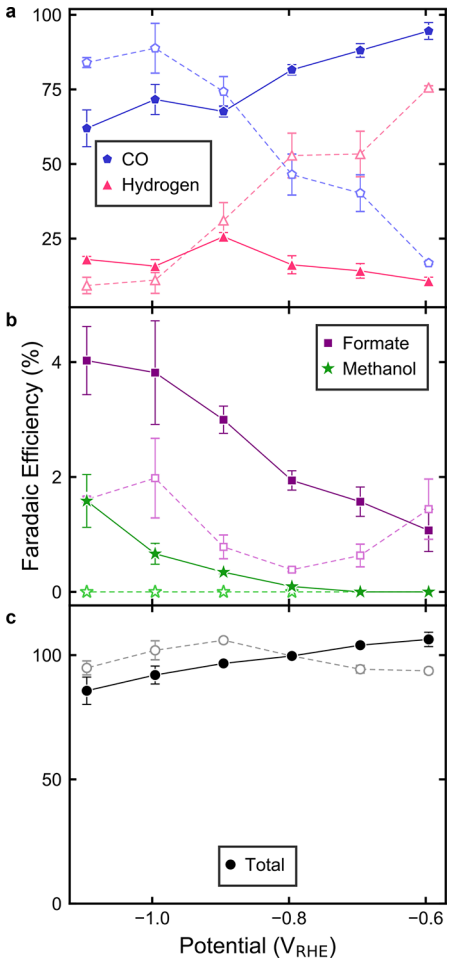

Figure 2. Faradaic efficiency for each product over an illuminated and dark silver cathode. Filled symbols with solid lines represent data collected under 365 nm LED illumination at 170 mW cm^{-2}. Open symbols with dashed lines represent data collected without illumination. (a) Faradaic efficiencies of carbon monoxide and hydrogen at a range of applied potentials. (b) Faradaic efficiencies of formate and methanol at a range of applied potentials. No methanol was detected in the dark. (c) Total Faradaic efficiencies at a range of applied potentials. Error bars represent the standard deviation of experiments performed in triplicate on three different electrodes.

The difference in product distributions between the illuminated and dark conditions is dramatic and dictated by the applied potential. At potentials more anodic than −0.9 V_{RHE}, the Faradaic efficiency and production rate of CO are significantly enhanced when the silver plasmonic catalyst is illuminated (Figures 2a and 3a). The most dramatic enhancement of CO occurs at the lowest potential used in this study, −0.6 V_{RHE}, where the Faradaic efficiency of carbon monoxide increases from 17% in the dark to 95% when the cathode is illuminated. The increase in CO Faradaic efficiency reflects a 3-, 5-, and 16-fold increase in the CO production rate in the light versus that in the dark at −0.8, −0.7, and −0.6 V_{RHE}, respectively (Figure 3a). The decrease in hydrogen Faradaic efficiency when the silver cathode is illuminated at these small cathodic potentials (Figure 2a) stems not only from the

DOI: 10.1021/acsenergylett.9b00515
ACS Energy Lett. 2019, 4, 1098−1105

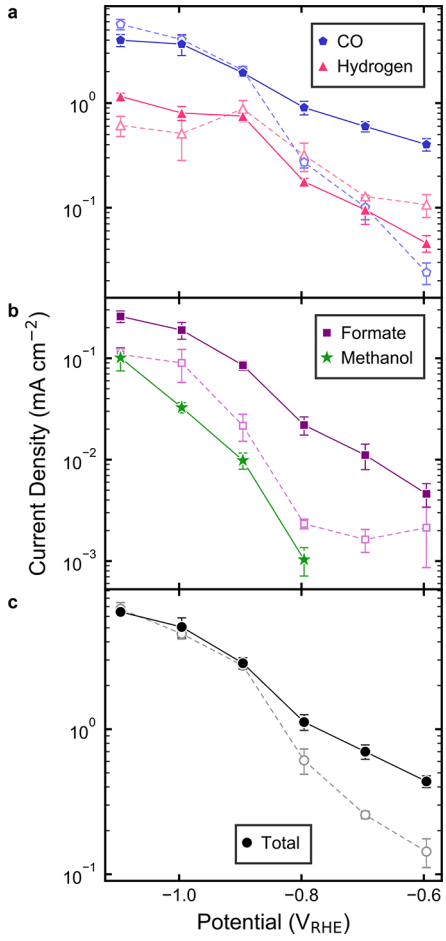

Figure 3. Tafel plot of the partial current density for each product over an illuminated and dark silver cathode. Filled symbols with solid lines represent data collected under 365 nm LED illumination at 170 mW cm^{-2}. Open symbols with dashed lines represent data collected without illumination. (a) Partial current densities of carbon monoxide and hydrogen at a range of applied potentials. (b) Partial current densities of formate and methanol at a range of applied potentials. No methanol was detected in the dark. (c) Total current densities at a range of applied potentials. Error bars represent the standard deviation of experiments performed in triplicate on three different electrodes.

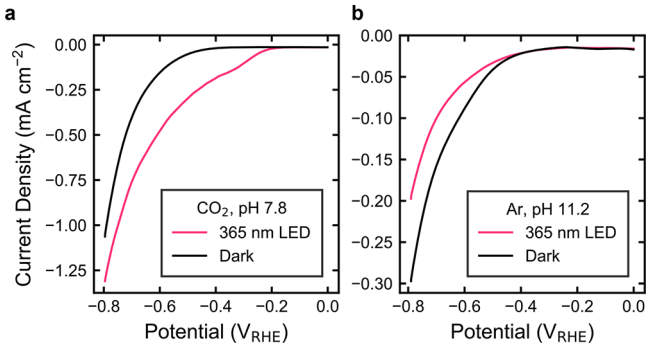

Figure 4. Cathodic voltage sweep at 100 mV s^{-1} at an illuminated and dark silver electrode in (a) CO_2- and (b) Ar-saturated 0.5 M K_2CO_3 under 365 nm LED light at 170 mW cm^{-2}. The voltage ranges were selected to ensure that no silver oxidation occurred at the anodic limit and to include all potentials where a photoeffect is observed for CO and H_2 in CO_2-saturated electrolyte at the cathodic limit.

increase in CO production but also from a notably lower rate of hydrogen generation in the light at these potentials (Figure 3a).

The cathodic sweep of a cyclic voltammogram (CV) in CO_2-saturated 1 M $KHCO_3$ predictably shows increased cathodic current and a decreased onset potential when the silver electrode is illuminated (Figure 4a). CO is the only product detected over the illuminated silver electrode at −0.37 V_{RHE}, while no products were detected at the same potential without illumination. CVs in Ar-saturated 0.5 M potassium carbonate (K_2CO_3) show the opposite trend—the cathodic current decreases under illumination relative to the unilluminated electrode (Figure 4b). Though the same starting electrolyte was used in both the Ar- and CO_2-saturated CVs, the presence of CO_2 lowers the pH, as noted in the legends of Figure 4. Similar results are observed in CO_2- and Ar-saturated 0.5 M sodium perchlorate ($NaClO_4$) (Figure S4), indicating that a plasmon interaction with adsorbed bicarbonate (which could plausibly be adsorbed to, and therefore block, active sites) is likely not impacting these results. Therefore, hydrogen production is suppressed on a plasmonic silver electrode regardless of the presence of CO_2 or specific electrolyte anions.

A plausible explanation for this CO formation selectivity over hydrogen evolution is that the plasmonically generated hot electrons are selectively, rather than indiscriminately, transferred to molecules adsorbed on the metal surface. In the case of plasmonic electrochemical CO_2 reduction, there are several leading theories for the mechanism of plasmonic hot-electron-driven photocatalysis that may be valid in this photoelectrochemical system.[12−15,27,28] In an indirect charge transfer mechanism, SPR excites a hot electron in the silver catalyst; subsequently, that hot electron is transferred to unoccupied molecular orbitals of an adsorbate. In a direct charge transfer mechanism, SPR induces direct charge transfer in the metal−adsorbate complex from an electronic state with primarily silver character to a hybridized orbital with primarily CO_2 reduction intermediate character.[27,28] In a transient negative ion (TNI) mechanism, plasmonic hot electrons are generated on the silver, populate unoccupied adsorbate states for a short time, and then return to the metal, leaving the adsorbate molecule in a vibrationally excited state with increased reactivity.[12−15] These three mechanisms are all consistent with the transfer of electron density to adsorbed CO_2 or an intermediate in the pathway to selectively form CO, formate, or methanol, as observed in this study.

The plasmonic suppression of hydrogen evolution superficially appears to be a completely different process than the promotion of CO_2 reduction. However, it is possible that hydrogen is suppressed because protons (or hydroxide ions) or water molecules are selectively purged from the surface of the silver electrode through desorption induced by electronic transitions (DIET), the basis for the TNI mechanism discussed above.[15,29] In the DIET mechanism, the hydrogen precursor is excited electronically through the transient population of unoccupied adsorbate orbitals. The DIET mechanism diverges from the TNI mechanism in the result of the vibrational excitation. In DIET, the adsorbate overcomes the surface binding energy and desorbs rather than overcoming a reaction barrier. Another possible explanation for hydrogen suppression is that the plasmonic hot electron populates a hybridized antibonding orbital in the metal−adsorbate complex. These

DOI: 10.1021/acsenergylett.9b00515
ACS Energy Lett. 2019, 4, 1098−1105

mechanisms share the common theme of inhibition of a critical intermediate in hydrogen generation.

In the case of CO_2, the interaction with a plasmonic catalyst spurs reaction, while the interaction of hydrogen precursors leads to a reversion to the initial state. Further studies are needed to distinguish among the proposed mechanisms, but the observation of differing interactions among adsorbates in the same catalytic system is unprecedented. Thus, plasmonic catalysis may allow the tuning of selectivity in complex reactions by promoting the surface reaction of some species and the depopulation of others.

At more cathodic potentials (−0.9 V_{RHE} and below), the differences in partial current density between light and dark conditions for hydrogen and carbon monoxide formation are small (Figure 3a). However, starting at −0.8 V_{RHE} and continuing to more cathodic potentials, the silver catalyst produces methanol when illuminated but no detectable methanol in the dark up to −1.1 V_{RHE} (Figures 2b and 3b). The initial detection of methanol in illuminated conditions at −0.8 V_{RHE} represents a 550 mV decrease in the required overpotential to produce methanol compared to a previous report of methanol production on unilluminated polycrystalline silver.[22] The rate of methanol production continues to increase at more cathodic potentials (Figure 3b), and the maximum methanol Faradaic efficiency achieved in this study is 1.4% when the cathode is illuminated and biased at −1.1 V_{RHE} (Figure 2b), which is more than 130 times greater than the methanol production efficiencies reported at a 250 mV higher overpotential on polycrystalline silver in dark conditions.[22] Given that methanol is the sole product that is only produced under illumination, we compare its partial current density at various wavelengths of constant photon flux (Figure 5). Partial current densities for other products at the same wavelengths show no obvious trends (Figure S5) likely due to the difficulty in deconvoluting dark and light currents. The methanol production rate at −1.1 V_{RHE} is proportional to the absorption of the conditioned silver electrode at the wavelength of illumination. The correlation between absorption and methanol production is a strong indication that methanol is generated via photonic effects. We present further evidence of photonic effects in later sections.

The formate production rate and Faradaic efficiency increase in the light relative to those in the dark from −1.1 to −0.7 V_{RHE} (Figures 2b and 3b). For example, in the potential window of −1.1 to −0.9 V_{RHE}, formate is produced under illumination at 2−4 times the rate of formate production at the same potential in the dark. The Faradaic efficiencies for all products reported for dark conditions here are in very good agreement with similar measurements reported by Hatsukade et al. on a polycrystalline silver foil electrode.[22]

Photocurrent Measurements. The photocurrent magnitude measured at constant voltage with 3 Hz light modulation (Figure 6a) grows with the magnitude of the applied cathodic potential (Figure 6b), in agreement with previous studies.[30] The maximum photocurrent of 0.62 mA cm^{-2} at −1.1 V_{RHE} represents an internal quantum efficiency of 4% for conversion of 170 mW cm^{-2} of 365 nm light. The difference in photocurrent at −1.1 V_{RHE} reported in Figure 6b and the photocurrent observed in Figure 6a results from the difference in CO_2 flow between the two measurements, resulting in different mass transport effects; CO_2 is sparged through the cell before the measurement in Figure 6a but stopped during data collection to reduce signal noise, whereas CO_2 is bubbled vigorously throughout in Figure 6b.

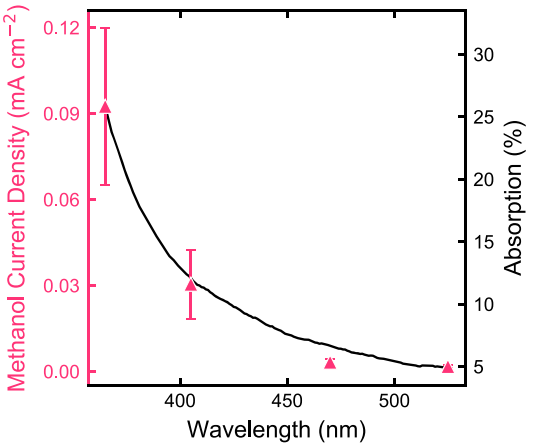

Figure 5. Methanol production rate under equal LED photon fluxes (3.2×10^{17} photons cm^{-2} s^{-1}) of different wavelengths (left ordinate) and absorption of the electrode (right ordinate) after performing CO_2 reduction at −1.1 V_{RHE} for 45 min. Absorption is calculated as 100% − %*R*, where %*R* is the total reflection measured by an integrating sphere.

In the potential window of −0.8 to −0.6 V_{RHE}, where CO production is plasmonically enhanced, the increase in CO partial current density at each potential (Figure 3a) is greater than the photocurrent density at the corresponding potential (Figure 6b). The decrease in hydrogen evolution (Figure 3a) at these potentials counteracts the promotion of CO, leading to a smaller than expected photocurrent. The rise in soluble product (formate and methanol) formation under illumination accounts for 14−41% of the photocurrent at potentials from −1.1 to −0.9 V_{RHE}. The remainder of the photocurrent likely modifies the production of CO and hydrogen slightly, although this production formation difference is not significant compared to statistical variation between trials. Notably, the difference between the total current density with and without illumination is also only statistically significant from −0.8 to −0.6 V_{RHE} (Figure 3c) where the photocurrent represents a relatively large proportion of the total current.

If plasmonically generated hot carriers are not extracted from the electrode, their excess energy is transferred to heating of other electrons, the lattice, and eventually the surroundings. SPR can be used to promote reactions by local heating, but the change in selectivity observed in this study cannot be explained by an increase in the local temperature at the cathode surface or heating from the LED. Our previous study showed that hydrogen production is enhanced and CO production is suppressed at elevated temperatures,[21] but hydrogen production rates remain the same or even decrease while CO production rates remain the same or increase with illumination in this study (Figures 3a and 4). This strongly suggests that localized plasmonic heating (if it is occurring) is not the source of the observed selectivity changes. The photocurrent on the silver electrode depends linearly on the incident 365 nm LED illumination intensities (Figure 6c), consistent with both an athermal mechanism for the photoactivity and the results shown in Figure 5.[8,31] No apparent trends are observed in light-intensity-dependent product analysis (Figure S6). The difference between the photocurrent reported for 170 mW cm^{-2} illumination with a 365 nm LED in Figure 6b,c is a result

DOI: 10.1021/acsenergylett.9b00515
ACS Energy Lett. 2019, 4, 1098−1105

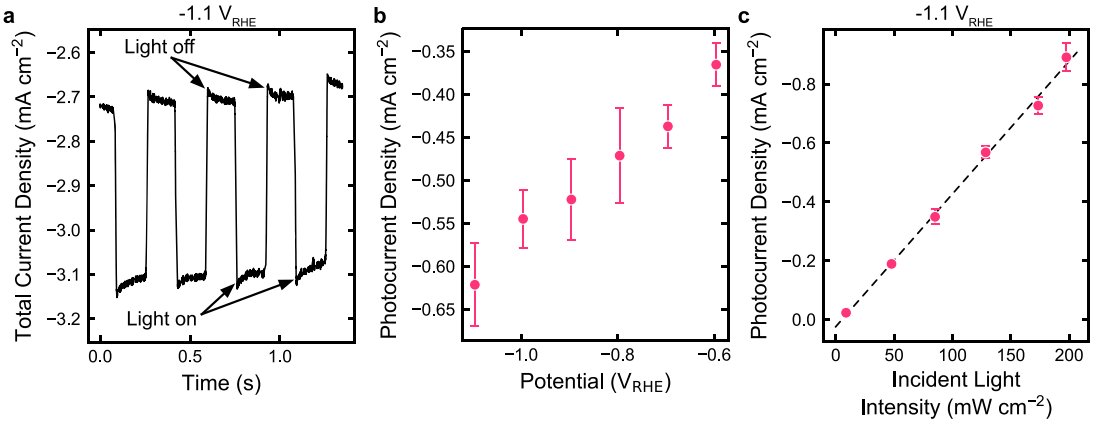

Figure 6. Photocurrent on silver cathodes under 170 mW cm^{-2} incident light intensity from a 365 nm LED. (a) Chopped-light chronoamperometry at −1.1 V_{RHE} over a silver cathode without CO_2 bubbling to decrease the noise in the signal. (b) Photocurrent density at various potentials. (c) Photocurrent density at various light intensities incident on the silver cathode at −1.1 V_{RHE}. The dotted line represents the least-squares regression line. Error bars in each figure represent the standard deviation of experiments performed in triplicate.

of slight experimental variations. The trends shown here are repeatable across all trials.

In this study, we find that a simple electrochemically conditioned polycrystalline silver thin film exhibits strong plasmonic activity that is selective for three different CO_2 reduction products, depending on the applied potential. The same electrode simultaneously suppresses hydrogen evolution. These combined effects indicate that plasmonics can be used to achieve selectivity in aqueous electrochemical CO_2 reduction. The silver nanostructures that give rise to these effects are not intentionally structured but formed electrochemically under highly cathodic conditions, meaning that the heterogeneous nanostructures are stable for hours at those conditions for product evolution. This study motivates the need for further research into several unsolved questions as the mechanism for the plasmonic selectivity is unclear. Further spectroscopic and computational research is needed to determine the role of the local electric field and the mechanism for hot electron transfer into acceptor molecules. A different nanostructure size or shape distribution to alter the SPR absorption or hot carrier generation could change the CO_2 reduction selectivity or make the plasmonic nanostructure selective for a different reaction altogether. Plasmonic nanostructures likely exhibit potential-dependent activity and selectivity for other electrochemical redox reactions, but we do not know whether all reactions can be catalyzed plasmonically. We will gain further insight into these mechanisms with the development of plasmonic catalysts with improved photon-to-current efficiencies and enhanced selectivities for other complex electrochemical reactions.

METHODS

Experimental methods are described here in brief and in more detail in the Supporting Information.

Synthesis of Silver Cathodes, The silver thin film cathode was fabricated by e-beam evaporation of 5 nm of titanium on a clean glass slide and 200 nm of silver over the titanium. Except where noted, all silver cathodes were electrochemically conditioned at −1.1 V_{RHE} for 45 min in CO_2-saturated aqueous 1 M $KHCO_3$ before use. X-ray photoelectron spectroscopy (XPS) of the electrochemically conditioned silver electrodes indicates that only silver, and no titanium, is present at the electrode surface after the conditioning step.

Cathode Surface Imaging and Profiling. SEM images were acquired using a Thermo Scientific Quanta FEG 250 SEM. AFM measurements were performed with a commercial AFM system (Bruker Dimension Icon) using the PeakForce Quantitative Nanoscale Mechanical tapping mode under ambient conditions. UV−visible reflection measurements were collected on a Shimadzu SolidSpec-3700 UV−vis−NIR spectrophotometer equipped with an integrating sphere.

Photoelectrochemical Measurements. The electrolyte used in this study was CO_2-saturated aqueous 1 M $KHCO_3$ (pH 7.75) made by saturating 0.5 M K_2CO_3 with CO_2 for 10 min. IR-corrected measurements were performed with a Biologic SP-300 potentiostat in a gastight polyether ether ketone (PEEK) electrochemical compression cell.[21] A Ferrotec 72008/131/150B Peltier cooler, CPU heat sink with a fan, and proportional integral derivative (PID) controller held the catholyte at a constant 22.0 ± 0.1 °C. A Selemion AMV anion exchange membrane separated the catholyte and anolyte. CO_2 was continuously bubbled at 5 sccm through a glass frit at the bottom of the cell. Platinum foil was used as the water oxidation anode. An Innovative Instruments, Inc., LF-1 leak-free Ag/AgCl electrode was used as the potential reference, but all potentials were converted to and reported versus the reversible hydrogen electrode. CVs were performed in Ar- and CO_2-saturated 0.5 M K_2CO_3 or 0.5 M $NaClO_4$ at a sweep rate of 100 mV s^{-1}. The cathodic sweep of the 10th cycle is plotted in Figures 4 and S4, although the trends shown are representative of any cycle.

The cathode was illuminated from the front using a Mightex Systems LCS-0365-48-22 365 nm ultrahigh-power LED with 170 mW cm^{-2} (3.2×10^{17} photons cm^{-2} s^{-1}) light intensity incident on the cathode. Similar LEDs were used with wavelengths centered at 405, 470, and 530 nm. Manufacturer-provided LED emission spectra are provided in Figure S7. The incident power was measured with a Coherent PowerMax PM10 power meter connected to a Coherent LabMax-TOP power meter console. Photocurrent was extracted from 3 Hz chopped-light chronoamperometry measurements using a Stanford Research Systems SR850 lock-in amplifier and a ThorLabs SHB1 shutter system.

Electrochemical Surface Area Measurements. The ECSA was determined relative to the as-e-beam-evaporated electrode by measuring the capacitive charging current in CVs at seven

DOI: 10.1021/acsenergylett.9b00515
ACS Energy Lett. 2019, 4, 1098−1105

different scan rates in a non-Faradaic voltage region (Figure S1a). The capacitance is the *y*-intercept of the best-fit line of the charging current versus scan rate (Figure S1b). Each measured capacitance was divided by the capacitance of the as-deposited electrode to find the relative surface area. The relative ECSA measured over a 50 mV non-Faradaic region as a function of CO_2 electrolysis time is reported in Figure 1d.

CO_2 Reduction Product Measurements. Gaseous products of the electrochemical reactions were analyzed by an in-line Multiple Gas Analyzer #5 SRI Instruments GC equipped with a 12 ft HayeSep D (divinylbenzene) column, thermal conductivity detector (TCD), flame ionization detector (FID) with a methanizer, and argon carrier gas. For a single product analysis run, a constant potential was applied for 64 min with GC injections at 3, 15, 27, 39, 51, and 63 min. Product partial current densities and Faradaic efficiencies were computed for each injection from a calibration curve with at least three points for each gas type. The average values over the last five injections are reported here. Liquid products in the catholyte and anolyte were quantified after the electrolysis was complete by ^{1}H NMR spectroscopy on a Bruker Avance III 500 MHz magnet.[32]

■ ASSOCIATED CONTENT

Supporting Information

The Supporting Information is available free of charge on the ACS Publications website at DOI: 10.1021/acsenergylett.9b00515.

> Detailed experimental section; representative example of ECSA determination; AFM images of as-deposited and electrochemically conditioned silver electrodes; SEM images of as-deposited and electrochemically conditioned silver electrodes; and cyclic voltammograms in $NaClO_4$, partial current density for each product at a range of illumination wavelengths and at a range of light intensities, and spectra for the LEDs used in this study (PDF)

■ AUTHOR INFORMATION

Corresponding Author

*E-mail: bmcclosk@berkeley.edu. Phone: (510) 642-2295. Address: Department of Chemical & Biomolecular Engineering, 201 Gilman Hall, University of California, Berkeley, CA 94720.

ORCID

Erin B. Creel: 0000-0002-4649-2018
Elizabeth R. Corson: 0000-0003-2722-674X
Bryan D. McCloskey: 0000-0001-6599-2336

Author Contributions

E.B.C. and E.R.C. performed the photoelectrochemical experiments and electrochemical surface area measurements. E.B.C. measured the UV−visible spectra, analyzed the product analysis data, created the figures, and wrote the manuscript. E.R.C. performed and analyzed the NMR experiments and SEM. J.E. performed and analyzed the AFM measurements. E.R.C., J.E., R.K., J.J.U., and B.D.M. edited the manuscript. B.D.M., J.J.U., and R.K. supervised the project.

Notes

The authors declare no competing financial interest.

■ ACKNOWLEDGMENTS

We thank E. Zaia for XPS measurements. We thank D. Perez, A. Buckley, G. Segev, J. Cooper, R. Creel, Gurudayal, D. Larson, and Y. Lum for useful discussions. This work was supported largely by the National Science Foundation under Grant No. CBET-1653430. This material is based upon work performed by the Joint Center for Artificial Photosynthesis, a DOE Energy Innovation Hub, supported through the Office of Science of the U.S. Department of Energy under Award No. DE-SC0004993. Work at the Molecular Foundry was supported by the Office of Science, Office of Basic Energy Sciences of the U.S. Department of Energy under Contract No. DE-AC02-05CH11231. E.R.C. and E.B.C. acknowledge support from the National Science Foundation Graduate Research Fellowship under Grant No. DGE 1106400.

■ REFERENCES

(1) Intergovernmental Panel on Climate Change, 2013. *The Physical Science Basis. Contribution of Working Group I to the Fifth Assessment Report of the Intergovernmental Panel on Climate Change*; Stocker, T. F., Qin, D., Plattner, G.-K., Tignor, M. M. B., Allen, S. K., Boschung, J., Nauels, A., Xia, Y., Bex, V., Midgley, P. M., Eds.; IPCC, Cambridge University Press: Cambridge and New York, 2013. DOI: 10.1029/2000JD000115.

(2) Hori, Y. Electrochemical CO_2 Reduction on Metal Electrodes. In *Modern Aspects of Electrochemistry*; Vayenas, C. G., White, R. E., Gamboa-Aldeco, M. E., Eds.; Springer: New York, 2008; Chapter 3, pp 89−189. DOI: 10.1007/978-0-387-49489-0_3.

(3) White, J. L.; Baruch, M. F.; Pander, J. E.; Hu, Y.; Fortmeyer, I. C.; Park, J. E.; Zhang, T.; Liao, K.; Gu, J.; Yan, Y.; et al. Light-Driven Heterogeneous Reduction of Carbon Dioxide: Photocatalysts and Photoelectrodes. *Chem. Rev.* **2015**, *115* (23), 12888−12935.

(4) Yu, S.; Wilson, A. J.; Kumari, G.; Zhang, X.; Jain, P. K. Opportunities and Challenges of Solar-Energy-Driven Carbon Dioxide to Fuel Conversion with Plasmonic Catalysts. *ACS Energy Lett.* **2017**, *2* (9), 2058−2070.

(5) Thomann, I.; Pinaud, B. A.; Chen, Z.; Clemens, B. M.; Jaramillo, T. F.; Brongersma, M. L. Plasmon Enhanced Solar-to-Fuel Energy Conversion. *Nano Lett.* **2011**, *11* (8), 3440−3446.

(6) Lee, J.; Mubeen, S.; Ji, X.; Stucky, G. D.; Moskovits, M. Plasmonic Photoanodes for Solar Water Splitting with Visible Light. *Nano Lett.* **2012**, *12* (9), 5014−5019.

(7) Ingram, D. B.; Linic, S. Water Splitting on Composite Plasmonic-Metal/Semiconductor Photoelectrodes: Evidence for Selective Plasmon-Induced Formation of Charge Carriers near the Semiconductor Surface. *J. Am. Chem. Soc.* **2011**, *133*, 5202−5205.

(8) Mukherjee, S.; Zhou, L.; Goodman, A. M.; Large, N.; Ayala-Orozco, C.; Zhang, Y.; Nordlander, P.; Halas, N. J. Hot-Electron-Induced Dissociation of H_2 on Gold Nanoparticles Supported on SiO_2. *J. Am. Chem. Soc.* **2014**, *136* (1), 64−67.

(9) Hou, W.; Hung, W. H.; Pavaskar, P.; Goeppert, A.; Aykol, M.; Cronin, S. B. Photocatalytic Conversion of CO_2 to Hydrocarbon Fuels via Plasmon-Enhanced Absorption and Metallic Interband Transitions. *ACS Catal.* **2011**, *1* (8), 929−936.

(10) Kumari, G.; Zhang, X.; Devasia, D.; Heo, J.; Jain, P. K. Watching Visible Light-Driven CO_2 Reduction on a Plasmonic Nanoparticle Catalyst. *ACS Nano* **2018**, *12*, 8330−8340.

(11) Yu, S.; Wilson, A. J.; Heo, J.; Jain, P. K. Plasmonic Control of Multi-Electron Transfer and C-C Coupling in Visible-Light-Driven CO_2 Reduction on Au Nanoparticles. *Nano Lett.* **2018**, *18* (4), 2189−2194.

(12) Kale, M. J.; Avanesian, T.; Christopher, P. Direct Photocatalysis by Plasmonic Nanostructures. *ACS Catal.* **2014**, *4* (1), 116−128.

(13) Brongersma, M. L.; Halas, N. J.; Nordlander, P. Plasmon-Induced Hot Carrier Science and Technology. *Nat. Nanotechnol.* **2015**, *10* (1), 25−34.

DOI: 10.1021/acsenergylett.9b00515
ACS Energy Lett. 2019, 4, 1098−1105

(14) Aslam, U.; Rao, V. G.; Chavez, S.; Linic, S. Catalytic Conversion of Solar to Chemical Energy on Plasmonic Metal Nanostructures. *Nat. Catal.* **2018**, *1* (9), 656.
(15) Linic, S.; Christopher, P.; Ingram, D. B. Plasmonic-Metal Nanostructures for Efficient Conversion of Solar to Chemical Energy. *Nat. Mater.* **2011**, *10* (12), 911−921.
(16) Marimuthu, A.; Zhang, J.; Linic, S. Tuning Selectivity in Propylene Epoxidation by Plasmon Mediated Photo-Switching of Cu Oxidation State. *Science* **2013**, *339* (6127), 1590−1593.
(17) Robatjazi, H.; Zhao, H.; Swearer, D. F.; Hogan, N. J.; Zhou, L.; Alabastri, A.; McClain, M. J.; Nordlander, P.; Halas, N. J. Plasmon-Induced Selective Carbon Dioxide Conversion on Earth-Abundant Aluminum-Cuprous Oxide Antenna-Reactor Nanoparticles. *Nat. Commun.* **2017**, *8* (1), 1−9.
(18) Zhang, X.; Li, X.; Zhang, D.; Su, N. Q.; Yang, W.; Everitt, H. O.; Liu, J. Product Selectivity in Plasmonic Photocatalysis for Carbon Dioxide Hydrogenation. *Nat. Commun.* **2017**, *8*, 14542.
(19) Duchene, J. S.; Tagliabue, G.; Welch, A. J.; Cheng, W. H.; Atwater, H. A. Hot Hole Collection and Photoelectrochemical CO_2 Reduction with Plasmonic Au/p-GaN Photocathodes. *Nano Lett.* **2018**, *18* (4), 2545−2550.
(20) Kostecki, R.; Augustynski, J. Electrochemical Reduction of CO_2 at an Activated Silver Electrode. *Berichte der Bunsengesellschaft fur Phys. Chemie* **1994**, *98* (12), 1510−1515.
(21) Corson, E. R.; Creel, E. B.; Kim, Y.; Urban, J. J.; Kostecki, R.; McCloskey, B. D. A Temperature-Controlled Photoelectrochemical Cell for Quantitative Product Analysis. *Rev. Sci. Instrum.* **2018**, *89* (5), 055112.
(22) Hatsukade, T.; Kuhl, K. P.; Cave, E. R.; Abram, D. N.; Jaramillo, T. F. Insights into the Electrocatalytic Reduction of CO_2 on Metallic Silver Surfaces. *Phys. Chem. Chem. Phys.* **2014**, *16* (27), 13814−13819.
(23) Maier, S. A. *Plasmonics: Fundamentals and Applications*; Springer: New York, 2007. DOI: 10.1016/j.aca.2010.06.020.
(24) Sundararaman, R.; Narang, P.; Jermyn, A. S.; Goddard, W. A., III; Atwater, H. A. Theoretical Predictions for Hot-Carrier Generation from Surface Plasmon Decay. *Nat. Commun.* **2014**, *5*, 5788.
(25) Vreeland, E. C.; Watt, J.; Schober, G. B.; Hance, B. G.; Austin, M. J.; Price, A. D.; Fellows, B. D.; Monson, T. C.; Hudak, N. S.; Maldonado-Camargo, L.; et al. Enhanced Nanoparticle Size Control by Extending LaMer's Mechanism. *Chem. Mater.* **2015**, *27* (17), 6059−6066.
(26) Alonso, C. The Evaluation of Surface Diffusion Coefficients of Gold and Platinum Atoms at Electrochemical Interfaces from Combined STM-SEM Imaging and Electrochemical Techniques. *J. Electrochem. Soc.* **1990**, *137* (7), 2161.
(27) Boerigter, C.; Campana, R.; Morabito, M.; Linic, S. Evidence and Implications of Direct Charge Excitation as the Dominant Mechanism in Plasmon-Mediated Photocatalysis. *Nat. Commun.* **2016**, *7*, 10545.
(28) Boerigter, C.; Aslam, U.; Linic, S. Mechanism of Charge Transfer from Plasmonic Nanostructures to Chemically Attached Materials. *ACS Nano* **2016**, *10* (6), 6108−6115.
(29) Ho, W. Reactions at Metal Surfaces Induced by Femtosecond Lasers, Tunneling Electrons, and Heating. *J. Phys. Chem.* **1996**, *100* (31), 13050−13060.
(30) Kim, Y.; Creel, E. B.; Corson, E. R.; McCloskey, B. D.; Urban, J. J.; Kostecki, R. Surface-Plasmon-Assisted Photoelectrochemical Reduction of CO_2 and NO_3^- on Nanostructured Silver Electrodes. *Adv. Energy Mater.* **2018**, *8* (22), 1800363.
(31) Li, K.; Hogan, N. J.; Kale, M. J.; Halas, N. J.; Nordlander, P.; Christopher, P. Balancing Near-Field Enhancement, Absorption, and Scattering for Effective Antenna-Reactor Plasmonic Photocatalysis. *Nano Lett.* **2017**, *17* (6), 3710−3717.
(32) Kuhl, K. P.; Cave, E. R.; Abram, D. N.; Jaramillo, T. F. New Insights into the Electrochemical Reduction of Carbon Dioxide on Metallic Copper Surfaces. *Energy Environ. Sci.* **2012**, *5*, 7050−7059.

DOI: 10.1021/acsenergylett.9b00515
ACS Energy Lett. 2019, 4, 1098−1105